

Supporting Information for:

**Light-induced Water Oxidation Catalyzed by an Oxido-bridged
Triruthenium Complex with a Ru-O-Ru-O-Ru Motif**

Yuta Tsubonouchi,^{a,b,c} Shu Lin,^{a,c} Alexander R. Parent,^c Gary W. Brudvig,^{* b} and Ken Sakai^{* a,c,d}

^a Department of Chemistry, Faculty of Sciences, Kyushu University, Motooka 744, Nishi-ku, Fukuoka 819-0395, Japan

^b Department of Chemistry, Yale University, 225 Prospect Street, P.O. Box 208107, New Haven, Connecticut 06520-8107, United States

^c International Institute for Carbon-Neutral Energy Research (WPI-I2CNER), Kyushu University, Motooka 744, Nishi-ku, Fukuoka 819-0395, Japan

^d Center for Molecular Systems (CMS), Kyushu University, Motooka 744, Nishi-ku, Fukuoka 819-0395, Japan

Contents

Experimental details	S2-S4
Crystallographic details	S5-S6
Tables S1-S2	S7-S14
Figures S1-S18	S15-S26
Table S3	S27
Figures S19-S21	S28-S30
References	S31

Experimental Details

Synthesis

General.

All solvents and reagents were of the highest quality available and were used as received. **RuM**¹ and [Ru(bpy)₃](NO₃)₂·3H₂O² were prepared according to the literature procedures.

*Preparation of [$\{Ru^{III}(bda)(pic)_2(\mu-O)\}_2Ru^{IV}(pic)_2(H_2O)_2\}(PF_6)_2\cdot 2H_2O$ (**RuT**²⁺)*

RuM (23.0 mg, 42.7 μ mol) was suspended in 9 mL water. The suspension was stirred at room temperature under air until **RuM** was completely dissolved. The solution was left stirred for approximately 8 h and UV–Vis spectra were monitored periodically. When the band at 688 nm seemed to achieve a maximum value, the dark green solution was cooled in ice bath followed by addition of a saturated aqueous NaPF₆ solution (ca. 1 mL). The green precipitate was collected by filtration, washed with cold water and diethyl ether, and dried in vacuo. Yield 18.6 mg (10.6 μ mol, 74%). ¹H NMR (D₂O, 600 MHz): δ 8.46 (d, *J* = 6.4 Hz, 4H), 8.44–7.66 (br. m, 12H), 7.58 (d, *J* = 6.4 Hz, 8H), 6.80 (d, *J* = 5.5 Hz, 8H), 6.67 (d, *J* = 6.4 Hz, 4H), 2.25 (s, 6H), 2.22 (s, 12H). Elemental analysis calculated for C₆₀H₅₈F₁₂N₁₀O₁₂P₂Ru₃·2H₂O : C, 41.41; H, 3.59; N, 8.05. Found: C, 41.22; H, 3.54; N, 8.05.

*Preparation of single crystals of [**RuT**²⁺](BF₄)₂·8H₂O*

To a solution of **RuT**²⁺ prepared by air oxidation of **RuM** (2.0 mg, 3.7 μ mol) in 6 mL water, two drops of a saturated aqueous NaBF₄ solution were added. Green crystals suitable for X-ray crystallography were grown at 5 °C over 2 days.

*Preparation of single crystals of [**RuT**³⁺](S₂O₈)(BF₄)·12H₂O*

To a solution of **RuT**²⁺ prepared by air oxidation of **RuM** (3.5 mg, 6.5 μ mol) in 4 mL water, Na₂S₂O₈ solid (500 equiv.) was added. The resulting solution was stirred at room temperature while tracking the formation of **RuT**³⁺ by UV-Vis spectroscopy. When the band at 688 nm reached a minimum value, some drops of a saturated aqueous NaBF₄ solution were added. Brown crystals suitable for X-ray crystallography were grown at 5 °C over 5 days.

Measurements

Electronic absorption spectra were recorded on Varian Cary50 UV–Vis and Shimadzu UV-3600 spectrophotometers using a 1 cm path length quartz cuvette. ^1H NMR spectra were recorded on JEOL JNM-ESA 600 and Agilent DD2 400 MHz spectrometers using 3-(trimethylsilyl)propionic-2,2,3,3-d₄ acid sodium salt as an internal standard. Electrochemical experiments were performed using standard three-electrode measurements carried out on a Princeton Applied Research VersaSTAT-4. Cyclic voltammetry (CV) experiments were performed at room temperature in a one-compartment cell equipped with a glassy carbon working electrode, a Ag/AgCl reference electrode (+0.197 V vs, NHE), and a platinum wire as the auxiliary electrode. A scan rate of 100 mV/s and 0.1M borate buffer (pH 8) were used. The relative concentrations of **RuM** and **RuT²⁺(PF₆)₂** used for the CV experiments (1:2, Figures 3 and S9) were lower than those used for the photochemical oxygen assay (3:1, Figure S11) due to the low solubility of **RuM** in aqueous media and the instability of **RuT²⁺(PF₆)₂** in organic solvents.

Oxygen assay

Photochemical oxygen evolution monitored by GC (Figures 4, S10 and S11).

Photochemical oxygen production from water was analyzed by using an automatic GC H₂/O₂ monitoring system developed in our group. In this system, a continuous flow of Ar (10.0 mL/min, controlled by a STEC SEC-E40/PAC-D2 digital mass flow controller) is bubbled through a photolysis solution (10 mL) contained in a Pyrex vial (*ca.* 20 mL). The vent gas from the vial is introduced into a valve that allows the automatic injection of the sample gas onto the GC (Shimadzu GC-8A equipped with a molecular sieve 5 Å column of 2 m × 3 mm *i.d.*, at 30 °C). The injection of the sample gas is controlled by software developed by K.S., and the output signal from the thermal conductivity detector of the gas chromatograph is analyzed by the Shimadzu C-R8A integrator. Photolysis solutions were degassed with Ar for 30 min prior to photolysis. Photoirradiation was performed using an ILC Technology CERMAX LX-300 300 W Xe lamp equipped with a CM-1 cold mirror (400 < λ < 800 nm). The photolysis vial was immersed in a 20 °C water bath to remove IR radiation and to eliminate temperature effects.

Photochemical oxygen evolution monitored by oxygen electrode (Figure S12).

A YSI 5300A Clark-type electrode was used to measure changes in dissolved oxygen concentration. The electrode, secured in a Teflon tube, was inserted into a tight-fitting water jacketed glass vessel for constant temperature (20 °C). The glass vessel was charged with **RuT²⁺**, [Ru(bpy)₃](NO₃)₂·3H₂O and Na₂S₂O₈ in buffer (4.7 mL). Photolysis solutions were degassed with Ar for 30 min prior to photolysis. Photoirradiation was performed using an 150 W quartz halogen lamp (Dolan-jenner industries, Inc. Fiber-Lite High Intensity Illuminator series 180) equipped with a 400 nm long-pass filter and an IR cut filter (Transmission spectrum for a set of the filters is shown in Figure S18).

Thermal oxygen evolution monitored by oxygen electrode (Figure S17).

A YSI 5300A Clark-type electrode was used to measure changes in dissolved oxygen concentration. The electrode, secured in a Teflon tube, was inserted into a tight-fitting water-jacketed glass vessel for constant temperature (20 °C). Solutions were not deaerated prior to use. A solution of Na₂S₂O₈ in buffer (5.00 mL) was placed in the glass vessel, and the system was allowed to equilibrate until a stable baseline was attained. After the baseline had stabilized, 250 μL of **RuT**²⁺ solution was injected into the glass vessel.

Crystallographic details

Refinement Details for $[\text{RuT}^{2+}](\text{BF}_4)_2 \cdot 8\text{H}_2\text{O}$

Low-temperature diffraction data were collected on a Bruker SMART APEXII CCD area detector diffractometer with the detector positioned at a distance of 6.0 cm from the crystal. The X-ray source was a monochromated Mo-K α radiation ($\lambda = 0.71073 \text{ \AA}$) from a rotating anode with a mirror focusing apparatus operated at 1.2 kW (50 kV, 24 mA). Corrections for absorption were made by SADABS.³ The structure was solved with SHELXS-97, and refined anisotropically on F^2 with SHELXL-97,⁴ where KENX⁵ was used to assist all the refinement procedures and to generate publication materials. All hydrogen atoms, except for those of the water solvate, were located in their idealized positions and included in the refinement using a riding model. Hydrogen atoms of the aqua ligand bound to the central Ru ion were located at the peak positions found in the difference Fourier map and were refined isotropically. Hydrogen atoms of water solvates were not located. Part of the water solvates could not be located. The crystal graphics were worked on by using DIAMOND.

The trimeric structure has a crystallographic inversion center at the central Ru ion. One of the carboxylate units does not coordinate to the ruthenium ion, and this unit shows nearly an identical C-O distance (O3-C32 = 1.245(5) and O5-C32 = 1.260(5) \AA), from which we confirmed the deprotonated nature of this unit. Including a BF_4^- anion found in the asymmetric unit, the compound is judged to have a Ru(III)₂Ru(IV) oxidation state. The diamagnetic character of this complex further supported this assignment. Moreover, the centrosymmetric feature further revealed that the compound has a Ru(III)-O-Ru(IV)-O-Ru(III) oxidation state in the crystal.

Refinement Details for $[\text{RuT}^{3+}](\text{S}_2\text{O}_8)(\text{BF}_4) \cdot 12\text{H}_2\text{O}$

Low-temperature diffraction data (ω -scans) were collected on a Rigaku R-Axis Spider diffractometer (sealed tube) coupled to a Rigaku R_AXIS RAPID imaging plate Mo K α ($\lambda = 0.71073 \text{ \AA}$) for the structure of RuT^{3+} . The diffraction images were processed and scaled using the Rigaku CrystalClear software.⁶ The structure was solved with SHELXT and was refined against F^2 on all data by full-matrix least squares with SHELXL,⁷ where KENX⁵ was used to assist all the refinement procedures including locating the disordered models and to generate publication materials. All hydrogen atoms, except for those of the water solvate, were located in their idealized positions and included in the refinement using a riding model. The crystal graphics were worked on by using DIAMOND.

The trimeric structure does not formally possess a crystallographic inversion center but is considered to possess a pseudo centrosymmetric structure as demonstrated in Table S3 and Figures S19 and S20. In the same manner as observed for RuT^{2+} , one of the carboxylate units of each bda ligand is not bound to the ruthenium ion, and possesses nearly an identical C-O distance (O7-C18 =

1.263(13), O8-C18 = 1.238(13), O11-C38 = 1.261(14), and O12-C38 = 1.242(13) Å), revealing that it is in the deprotonated form serving as one of the counter anions for the complex. The two oxygen donors bound to the central Ru ion were reasonably judged both as aqua ligands based on the good similarity of the coordinate bonds between the \mathbf{RuT}^{2+} and \mathbf{RuT}^{3+} cations (see Figure S20). As described above, the asymmetric unit includes two unligated carboxylate units, a BF_4^- anion, and a $\text{S}_2\text{O}_8^{2-}$ dianion, the overall charge can be judged as proposed with its chemical formula. By including two carboxylate donors from two bda's as well as two oxido donors bridging the three Ru ions, the oxidation state of Ru(III)Ru(IV)_2 proposed can be reasonably deduced. Moreover, as evidenced by the pseudo centrosymmetric feature of this trimer (see Table S3, and Figures S19-S21), the compound may be classified as a so-called Robin-Day Class III delocalized mixed-valence compound, which may be described as having a $\text{Ru(3.5+)-O-Ru(4.0+)-O-Ru(3.5+)}$ oxidation state in the crystal, although crystallographic disorder cannot be ruled out as the origin of the equivalent structures of the two terminal Ru ions.

Table S1. Crystal data collection and structure refinement parameters for $[\text{RuT}^{2+}](\text{BF}_4)_2 \cdot 8\text{H}_2\text{O}$ and $[\text{RuT}^{3+}](\text{S}_2\text{O}_8)(\text{BF}_4) \cdot 12\text{H}_2\text{O}$.

	$[\text{RuT}^{2+}](\text{BF}_4)_2 \cdot 8\text{H}_2\text{O}$	$[\text{RuT}^{3+}](\text{S}_2\text{O}_8)(\text{BF}_4) \cdot 12\text{H}_2\text{O}$
formula	$\text{C}_{60}\text{H}_{74}\text{B}_2\text{F}_8\text{N}_{10}\text{O}_{20}\text{Ru}_3$	$\text{C}_{60}\text{H}_{82}\text{BF}_4\text{N}_{10}\text{O}_{32}\text{Ru}_3\text{S}_2$
fw	1732.12	1909.50
color, habit	green, prisms	brown, prisms
crystal size, mm	0.25x0.20x0.17	0.3x0.2x0.2
crystal system	Monoclinic	Triclinic
space group	$P 2_1/n$ (No. 14)	$P -1$ (No. 2)
a, Å	14.515(5)	15.229(3)
b, Å	14.999(5)	17.001(3)
c, Å	15.692(5)	17.204(3)
α , deg	90.00	65.62(3)
β , deg	96.150(5)	84.91(3)
γ , deg	90.00	71.63(3)
V, Å ³	3396.6(19)	3846.1(13)
Z	2	2
F(000)	1756	1946
d_{calc} , g/cm ³	1.694	1.649
$\mu(\text{Mo K}\alpha)$, mm ⁻¹	0.761	0.737
T, K	100(2)	100(2)
radiation, Å	0.71073	0.71073
θ range, deg	$1.82 < \theta < 25.30$	$3.02 < \theta < 19.98$
index ranges	$-17 < h < 17, -17 < k < 17, -18 < l < 18$	$-14 < h < 14, -16 < k < 16, -16 < l < 16$
reflns measd	33103	50447
uniq reflns	6158	7140
R(int)	0.1028	0.1279
data/restraints/params	6158/0/494	7140/44/1037
R1 [$I \geq 2\sigma(I)$]	0.0412	0.0598
wR2 (all data)	0.0979 ^a	0.1657 ^b
GOF	1.019	1.086
max/mean shift/esd	0.001/0.000	0.010/0.000
max/min diff. peaks	1.160/-0.484	1.138/-0.596

^a $w=1/[\sigma^2(\text{F}_o^2)+(0.0272\text{P})^2+5.5635\text{P}]$ where $\text{P}=(\text{F}_o^2+2\text{F}_c^2)/3$. ^b $w=1/[\sigma^2(\text{F}_o^2)+(0.0679\text{P})^2+25.384\text{P}]$ where $\text{P}=(\text{F}_o^2+2\text{F}_c^2)/3$.

Table S2. Interatomic Distances (Å) and Angles (deg) for $[\text{RuT}^{2+}](\text{BF}_4)_2 \cdot 8\text{H}_2\text{O}$ and $[\text{RuT}^{3+}](\text{S}_2\text{O}_8)(\text{BF}_4) \cdot 12\text{H}_2\text{O}$.

$[\text{RuT}^{2+}](\text{BF}_4)_2 \cdot 8\text{H}_2\text{O}$

Ru1-O4	1.903(3)	Ru1-N1	1.987(3)
Ru1-O2	2.080(3)	Ru1-N3	2.088(3)
Ru1-N4	2.114(3)	Ru1-N2	2.123(3)
Ru2-O4 ^a	1.812(3)	Ru2-O4	1.812(3)
Ru2-O6 ^a	2.072(3)	Ru2-O6	2.072(3)
Ru2-N5 ^a	2.100(3)	Ru2-N5	2.100(3)
F1-B1	1.358(8)	F2A-F2B	0.85(6)
F2A-B1	1.358(11)	F2B-B1	1.58(3)
F3-B1	1.396(8)	F4-B1	1.394(8)
O1-C12	1.228(5)	O2-C12	1.294(5)
O3-C32	1.245(5)	O5-C32	1.260(5)
O10A-O10B	0.952(17)	N1-C11	1.344(5)
N1-C7	1.352(5)	N2-C2	1.340(5)
N2-C6	1.381(5)	N3-C17	1.341(5)
N3-C13	1.357(5)	N4-C23	1.343(6)
N4-C19	1.349(6)	N5-C26	1.347(5)
N5-C30	1.347(5)	C2-C3	1.392(6)
C2-C32	1.517(6)	C3-C4	1.379(6)
C4-C5	1.390(6)	C5-C6	1.382(6)
C6-C7	1.463(6)	C7-C8	1.393(6)
C8-C9	1.387(6)	C9-C10	1.391(6)
C10-C11	1.379(6)	C11-C12	1.509(6)
C13-C14	1.374(6)	C14-C15	1.397(6)
C15-C16	1.385(6)	C15-C18	1.498(6)
C16-C17	1.375(6)	C19-C20	1.379(6)
C20-C24	1.384(7)	C22-C24	1.381(7)
C22-C23	1.384(6)	C24-C25	1.503(6)
C26-C27	1.382(6)	C27-C28	1.387(6)
C28-C29	1.389(6)	C28-C31	1.502(6)
C29-C30	1.377(6)		

O4-Ru1-N1	171.56(13)	O4-Ru1-O2	92.67(11)
N1-Ru1-O2	78.93(12)	O4-Ru1-N3	89.95(12)
N1-Ru1-N3	90.20(13)	O2-Ru1-N3	85.59(12)
O4-Ru1-N4	90.56(12)	N1-Ru1-N4	88.50(13)
O2-Ru1-N4	88.94(13)	N3-Ru1-N4	174.53(13)
O4-Ru1-N2	110.20(12)	N1-Ru1-N2	78.19(13)
O2-Ru1-N2	157.12(12)	N3-Ru1-N2	95.02(13)
N4-Ru1-N2	89.92(13)	O4 ^a -Ru2-O4	180.00(15)
O4 ^a -Ru2-O6 ^a	89.45(13)	O4-Ru2-O6 ^a	90.55(13)
O4 ^a -Ru2-O6	90.55(13)	O4-Ru2-O6	89.45(13)
O6 ^a -Ru2-O6	180.0	O4 ^a -Ru2-N5 ^a	89.19(13)
O4-Ru2-N5 ^a	90.81(13)	O6 ^a -Ru2-N5 ^a	86.91(13)
O6-Ru2-N5 ^a	93.09(13)	O4 ^a -Ru2-N5	90.81(13)
O4-Ru2-N5	89.19(13)	O6 ^a -Ru2-N5	93.09(13)
O6-Ru2-N5	86.91(13)	N5 ^a -Ru2-N5	180.000(1)
F2B-F2A-B1	88.0(18)	F2A-F2B-B1	59.4(19)
C12-O2-Ru1	114.6(3)	Ru2-O4-Ru1	164.30(17)
C11-N1-C7	122.2(4)	C11-N1-Ru1	117.8(3)
C7-N1-Ru1	120.0(3)	C2-N2-C6	117.8(4)
C2-N2-Ru1	129.4(3)	C6-N2-Ru1	112.7(3)
C17-N3-C13	116.8(4)	C17-N3-Ru1	124.7(3)
C13-N3-Ru1	118.3(3)	C23-N4-C19	117.0(4)
C23-N4-Ru1	124.1(3)	C19-N4-Ru1	119.0(3)
C26-N5-C30	117.8(4)	C26-N5-Ru2	120.2(3)
C30-N5-Ru2	121.9(3)	N2-C2-C3	123.0(4)
N2-C2-C32	117.5(4)	C3-C2-C32	119.4(4)
C4-C3-C2	118.9(4)	C3-C4-C5	119.3(4)
C6-C5-C4	119.3(4)	N2-C6-C5	121.7(4)
N2-C6-C7	115.5(4)	C5-C6-C7	122.8(4)
N1-C7-C8	118.7(4)	N1-C7-C6	113.3(3)
C8-C7-C6	128.0(4)	C9-C8-C7	119.6(4)
C8-C9-C10	120.2(4)	C11-C10-C9	118.1(4)
N1-C11-C10	121.1(4)	N1-C11-C12	112.4(3)
C10-C11-C12	126.4(4)	O1-C12-O2	123.8(4)
O1-C12-C11	120.7(4)	O2-C12-C11	115.4(4)
N3-C13-C14	122.8(4)	C13-C14-C15	120.2(4)

C16-C15-C14	116.6(4)	C16-C15-C18	122.3(4)
C14-C15-C18	121.1(4)	C17-C16-C15	120.5(4)
N3-C17-C16	123.2(4)	N4-C19-C20	123.0(4)
C19-C20-C24	119.9(5)	C24-C22-C23	120.1(5)
N4-C23-C22	122.7(5)	C22-C24-C20	117.3(4)
C22-C24-C25	121.0(5)	C20-C24-C25	121.6(5)
N5-C26-C27	122.2(4)	C26-C27-C28	120.6(4)
C27-C28-C29	116.5(4)	C27-C28-C31	121.3(4)
C29-C28-C31	122.2(4)	C30-C29-C28	120.6(4)
N5-C30-C29	122.3(4)	O3-C32-O5	126.9(4)
O3-C32-C2	117.5(4)	O5-C32-C2	115.5(4)
F2A-B1-F1	104.2(14)	F2A-B1-F4	107.7(6)
F1-B1-F4	109.4(6)	F2A-B1-F3	117.6(15)
F1-B1-F3	108.5(5)	F4-B1-F3	109.2(6)
F2A-B1-F2B	32.6(18)	F1-B1-F2B	127.4(18)
F4-B1-F2B	112.2(12)	F3-B1-F2B	87(3)

[RuT³⁺](S₂O₈)(BF₄)•12H₂O

Ru1-O2	1.809(6)	Ru1-O1	1.817(7)
Ru1-O4	2.050(6)	Ru1-O3	2.068(7)
Ru1-N1	2.084(9)	Ru1-N2	2.110(9)
Ru2-O1	1.875(7)	Ru2-N5	2.009(8)
Ru2-O5	2.015(7)	Ru2-N3	2.070(9)
Ru2-N9	2.102(9)	Ru2-N4	2.123(9)
Ru3-O2	1.884(6)	Ru3-N10	2.006(9)
Ru3-O9	2.030(7)	Ru3-N7	2.067(9)
Ru3-N8	2.105(9)	Ru3-N6	2.123(9)
S1-O13	1.431(8)	S1-O14	1.432(8)
S1-O15	1.444(8)	S1-O16	1.652(8)
S2-O19	1.427(8)	S2-O18	1.441(8)
S2-O20	1.443(8)	S2-O17	1.658(8)
F1A-B3A	1.359(18)	F2A-B3A	1.359(19)
F3A-B3A	1.361(19)	F4A-B3A	1.350(18)
F1B-B3B	1.366(19)	F2B-B3B	1.387(19)

F3B-B3B	1.37(2)	F4B-B3B	1.37(2)
O5-C35	1.308(13)	O6-C35	1.216(13)
O7-C18	1.263(13)	O8-C18	1.238(13)
O9-C53	1.303(13)	O10-C53	1.243(13)
O11-C38	1.261(14)	O12-C38	1.242(13)
O16-O17	1.461(10)	N1-C1	1.348(13)
N1-C6	1.365(13)	N2-C46	1.353(13)
N2-C3	1.356(13)	N3-C16	1.349(14)
N3-C26	1.370(13)	N4-C28	1.360(13)
N4-C59	1.360(13)	N5-C14	1.332(13)
N5-C13	1.357(13)	N6-C11	1.333(14)
N6-C10	1.347(13)	N7-C29	1.346(13)
N7-C56	1.351(13)	N8-C22	1.363(13)
N8-C23	1.378(13)	N9-C36	1.355(13)
N9-C43	1.383(13)	N10-C39	1.340(13)
N10-C52	1.358(13)	C1-C2	1.382(15)
C2-C8	1.392(15)	C3-C4	1.379(15)
C4-C5	1.365(14)	C5-C7	1.404(14)
C5-C20	1.497(14)	C6-C9	1.364(14)
C7-C46	1.376(15)	C8-C9	1.391(15)
C8-C32	1.471(15)	C10-C27	1.382(15)
C11-C12	1.397(16)	C12-C21	1.380(16)
C13-C25	1.374(15)	C13-C35	1.486(16)
C14-C15	1.396(15)	C14-C43	1.485(15)
C15-C19	1.392(15)	C16-C17	1.398(15)
C17-C34	1.390(16)	C18-C36	1.536(15)
C19-C25	1.382(15)	C21-C27	1.356(15)
C21-C60	1.496(16)	C22-C30	1.386(15)
C22-C38	1.520(16)	C23-C24	1.381(14)
C23-C39	1.470(15)	C24-C31	1.370(15)
C26-C50	1.364(15)	C28-C49	1.389(15)
C29-C51	1.362(14)	C30-C31	1.367(15)
C33-C34	1.496(15)	C34-C50	1.368(16)
C36-C37	1.387(15)	C37-C45	1.369(15)
C39-C40	1.392(15)	C40-C41	1.392(15)
C41-C42	1.375(15)	C42-C52	1.362(15)

C43-C44	1.378(15)	C44-C45	1.371(15)
C47-C59	1.380(15)	C47-C48	1.381(16)
C48-C49	1.399(16)	C48-C58	1.479(15)
C51-C54	1.371(15)	C52-C53	1.478(16)
C54-C55	1.402(15)	C54-C57	1.503(15)
C55-C56	1.383(15)		
O2-Ru1-O1	179.5(3)	O2-Ru1-O4	90.1(3)
O1-Ru1-O4	90.3(3)	O2-Ru1-O3	89.8(3)
O1-Ru1-O3	89.8(3)	O4-Ru1-O3	179.7(3)
O2-Ru1-N1	88.0(3)	O1-Ru1-N1	91.8(3)
O4-Ru1-N1	93.1(3)	O3-Ru1-N1	86.6(3)
O2-Ru1-N2	91.0(3)	O1-Ru1-N2	89.2(3)
O4-Ru1-N2	87.3(3)	O3-Ru1-N2	93.0(3)
N1-Ru1-N2	178.9(4)	O1-Ru2-N5	171.4(3)
O1-Ru2-O5	93.3(3)	N5-Ru2-O5	78.2(3)
O1-Ru2-N3	88.8(3)	N5-Ru2-N3	90.9(3)
O5-Ru2-N3	86.0(3)	O1-Ru2-N9	111.2(3)
N5-Ru2-N9	77.3(4)	O5-Ru2-N9	155.4(3)
N3-Ru2-N9	91.8(3)	O1-Ru2-N4	92.0(3)
N5-Ru2-N4	87.8(3)	O5-Ru2-N4	90.7(3)
N3-Ru2-N4	176.7(3)	N9-Ru2-N4	90.9(3)
O2-Ru3-N10	170.5(3)	O2-Ru3-O9	92.8(3)
N10-Ru3-O9	77.9(3)	O2-Ru3-N7	88.1(3)
N10-Ru3-N7	89.6(3)	O9-Ru3-N7	86.7(3)
O2-Ru3-N8	111.6(3)	N10-Ru3-N8	77.7(4)
O9-Ru3-N8	155.5(3)	N7-Ru3-N8	92.4(3)
O2-Ru3-N6	94.1(3)	N10-Ru3-N6	87.6(3)
O9-Ru3-N6	88.9(3)	N7-Ru3-N6	175.2(3)
N8-Ru3-N6	90.8(3)	O13-S1-O14	115.9(5)
O13-S1-O15	114.9(5)	O14-S1-O15	113.7(5)
O13-S1-O16	97.5(4)	O14-S1-O16	106.0(4)
O15-S1-O16	106.5(4)	O19-S2-O18	114.7(5)
O19-S2-O20	115.1(5)	O18-S2-O20	115.3(5)
O19-S2-O17	105.2(4)	O18-S2-O17	96.9(4)
O20-S2-O17	106.9(4)	Ru1-O1-Ru2	165.2(4)

Ru1-O2-Ru3	164.1(4)	C35-O5-Ru2	118.0(7)
C53-O9-Ru3	116.4(7)	O17-O16-S1	108.0(5)
O16-O17-S2	108.1(5)	C1-N1-C6	116.2(9)
C1-N1-Ru1	121.8(7)	C6-N1-Ru1	122.0(8)
C46-N2-C3	117.8(10)	C46-N2-Ru1	123.7(8)
C3-N2-Ru1	118.5(8)	C16-N3-C26	116.5(10)
C16-N3-Ru2	118.0(8)	C26-N3-Ru2	125.5(8)
C28-N4-C59	117.1(10)	C28-N4-Ru2	122.7(7)
C59-N4-Ru2	120.2(8)	C14-N5-C13	122.3(9)
C14-N5-Ru2	120.3(7)	C13-N5-Ru2	117.4(7)
C11-N6-C10	115.2(10)	C11-N6-Ru3	123.6(8)
C10-N6-Ru3	121.0(8)	C29-N7-C56	115.9(9)
C29-N7-Ru3	119.1(7)	C56-N7-Ru3	124.9(8)
C22-N8-C23	116.1(9)	C22-N8-Ru3	129.3(7)
C23-N8-Ru3	114.7(7)	C36-N9-C43	115.8(9)
C36-N9-Ru2	129.0(7)	C43-N9-Ru2	115.2(7)
C39-N10-C52	121.9(9)	C39-N10-Ru3	119.4(7)
C52-N10-Ru3	118.6(8)	N1-C1-C2	123.0(10)
C1-C2-C8	120.9(11)	N2-C3-C4	121.2(10)
C5-C4-C3	122.1(10)	C4-C5-C7	116.2(10)
C4-C5-C20	122.1(10)	C7-C5-C20	121.7(10)
C9-C6-N1	122.6(11)	C46-C7-C5	120.4(10)
C2-C8-C9	115.2(10)	C2-C8-C32	122.1(11)
C9-C8-C32	122.7(11)	C6-C9-C8	121.9(11)
N6-C10-C27	123.5(11)	N6-C11-C12	123.6(11)
C21-C12-C11	120.1(11)	N5-C13-C25	119.9(10)
N5-C13-C35	112.1(10)	C25-C13-C35	127.9(11)
N5-C14-C15	120.0(10)	N5-C14-C43	113.7(10)
C15-C14-C43	126.3(10)	C19-C15-C14	118.2(11)
N3-C16-C17	122.6(11)	C34-C17-C16	119.8(11)
O8-C18-O7	128.2(11)	O8-C18-C36	117.7(11)
O7-C18-C36	114.1(11)	C25-C19-C15	120.5(11)
C27-C21-C12	116.1(11)	C27-C21-C60	123.9(12)
C12-C21-C60	120.0(12)	N8-C22-C30	121.9(10)
N8-C22-C38	118.5(10)	C30-C22-C38	119.6(10)
N8-C23-C24	123.2(10)	N8-C23-C39	113.9(9)

C24-C23-C39	122.8(10)	C31-C24-C23	119.0(10)
C13-C25-C19	119.1(11)	C50-C26-N3	122.7(11)
C21-C27-C10	121.3(11)	N4-C28-C49	122.4(11)
N7-C29-C51	123.6(10)	C31-C30-C22	120.5(11)
C30-C31-C24	119.0(11)	C50-C34-C17	117.0(10)
C50-C34-C33	122.6(12)	C17-C34-C33	120.4(11)
O6-C35-O5	123.9(11)	O6-C35-C13	121.8(11)
O5-C35-C13	114.3(10)	N9-C36-C37	123.1(10)
N9-C36-C18	116.9(10)	C37-C36-C18	119.9(10)
C45-C37-C36	119.1(10)	O12-C38-O11	129.2(11)
O12-C38-C22	114.9(12)	O11-C38-C22	115.9(11)
N10-C39-C40	119.2(10)	N10-C39-C23	114.2(9)
C40-C39-C23	126.6(11)	C41-C40-C39	119.4(11)
C42-C41-C40	119.4(11)	C52-C42-C41	119.9(11)
C44-C43-N9	123.1(10)	C44-C43-C14	123.6(10)
N9-C43-C14	113.4(9)	C45-C44-C43	118.9(10)
C37-C45-C44	119.8(10)	N2-C46-C7	122.2(10)
C59-C47-C48	121.6(11)	C47-C48-C49	116.2(11)
C47-C48-C58	122.4(11)	C49-C48-C58	121.2(12)
C28-C49-C48	120.6(11)	C26-C50-C34	121.4(11)
C29-C51-C54	120.9(10)	N10-C52-C42	120.1(10)
N10-C52-C53	110.4(10)	C42-C52-C53	129.5(11)
O10-C53-O9	122.1(11)	O10-C53-C52	121.4(12)
O9-C53-C52	116.4(11)	C51-C54-C55	116.9(10)
C51-C54-C57	122.4(10)	C55-C54-C57	120.7(11)
C56-C55-C54	119.0(10)	N7-C56-C55	123.6(11)
N4-C59-C47	122.2(11)	F4A-B3A-F1A	109.4(15)
F4A-B3A-F2A	108.9(14)	F1A-B3A-F2A	110.0(15)
F4A-B3A-F3A	109.9(15)	F1A-B3A-F3A	108.2(14)
F2A-B3A-F3A	110.4(15)	F1B-B3B-F3B	111.1(15)
F1B-B3B-F4B	110.7(15)	F3B-B3B-F4B	110.4(15)
F1B-B3B-F2B	108.3(15)	F3B-B3B-F2B	108.9(15)
F4B-B3B-F2B	107.3(15)		

^aSymmetry operation: 1-x, -y, 2-z.

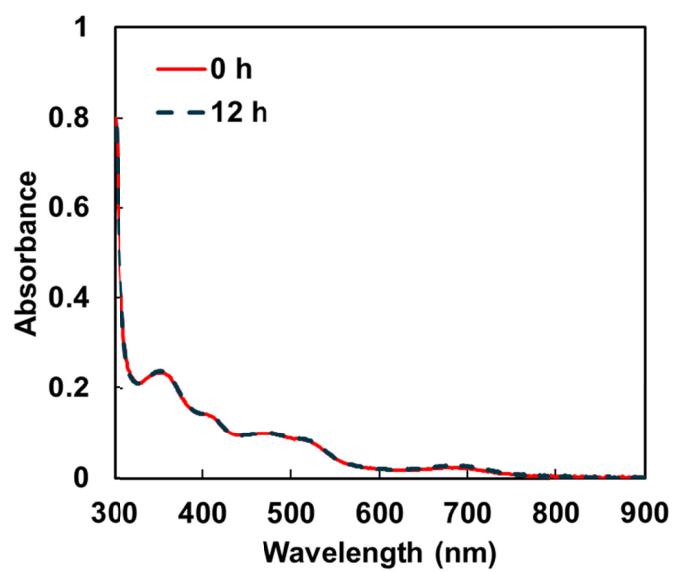


Figure S1. UV-Vis spectral time-course of 0.03 mM RuM in 0.1 M borate buffer (pH 8) under N₂.

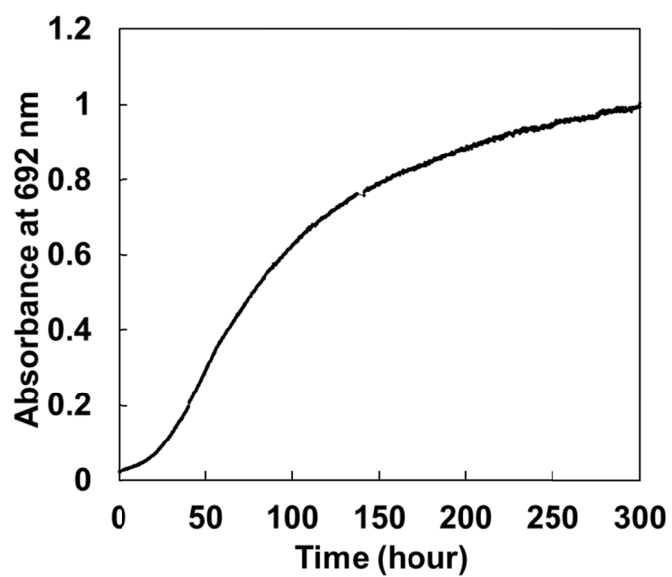


Figure S2. Time-dependent absorbance changes at 692 nm during oxidation of 0.03 mM RuM in 0.1 M borate buffer (pH 8) under air.

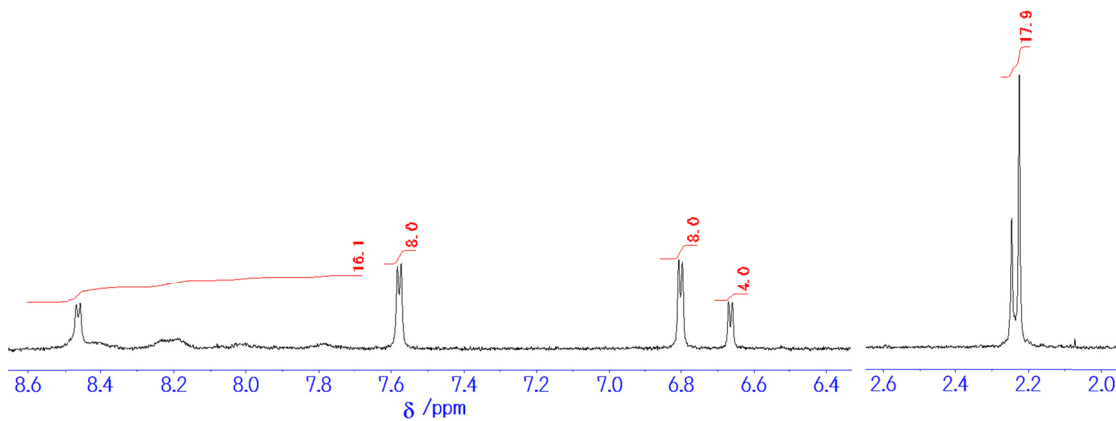


Figure S3. ^1H NMR spectrum of $\text{RuT}^{2+}(\text{PF}_6)_2$ in D_2O .

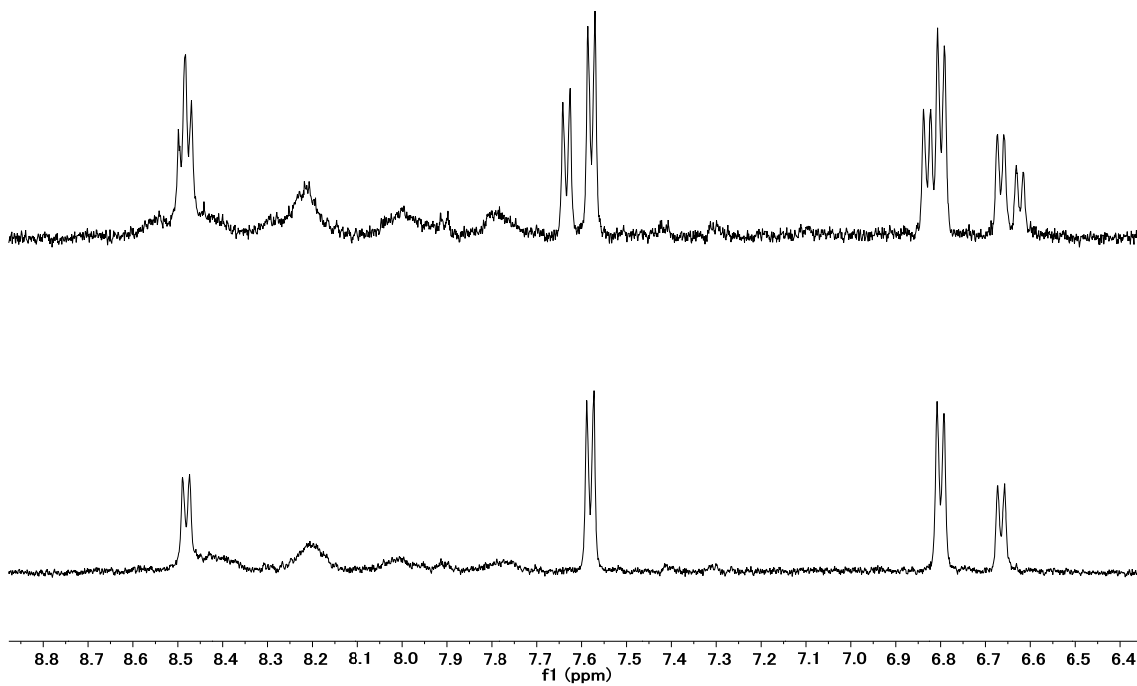


Figure S4. Partial ^1H NMR spectra of $\text{RuT}^{2+}(\text{PF}_6)_2$ in D_2O with NaCl (top) and without NaCl (bottom).

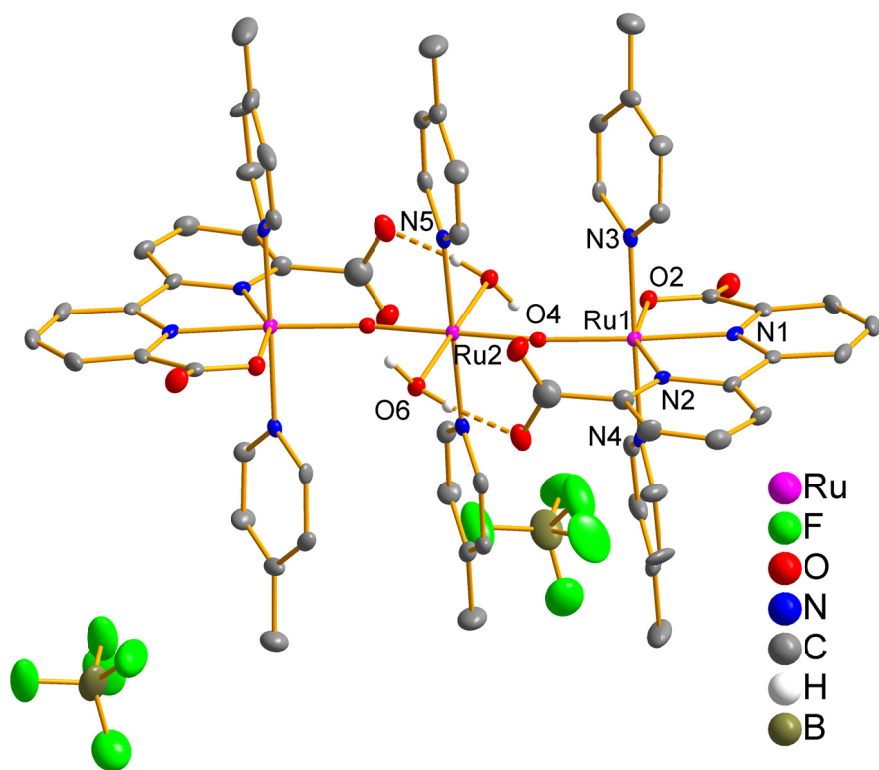


Figure S5. Crystal structure of $[\text{RuT}^{2+}](\text{BF}_4)_2 \cdot 8\text{H}_2\text{O}$. Hydrogen atoms except for those bonded to oxygen atoms are omitted for clarity. Hydrogen bonds are represented by dotted lines.

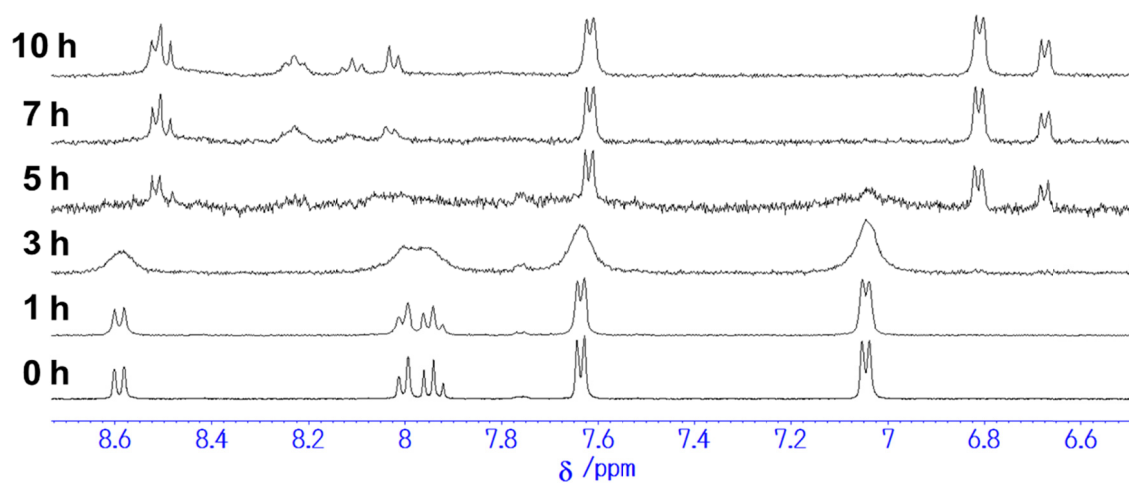


Figure S6. ¹H NMR time-course for the conversion of **RuM** to **RuT²⁺(PF₆)₂** in D₂O / acetone-d₆ (7.5 : 1).

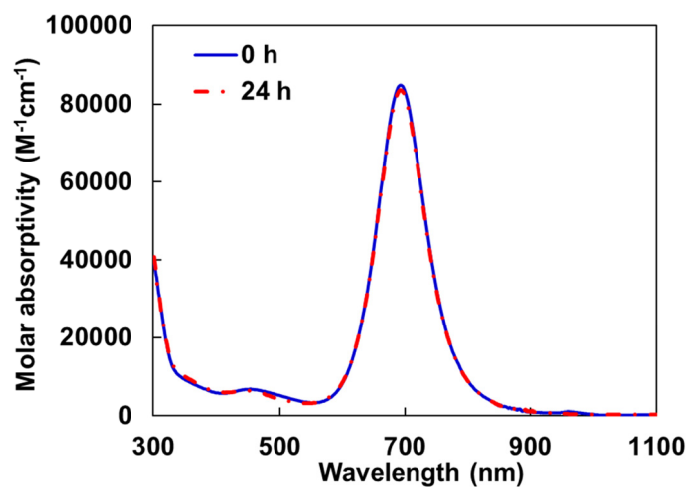


Figure S7. UV-Vis spectral time-course of 10 μM $\text{RuT}^{2+}(\text{PF}_6)_2$ in 0.1 M borate buffer (pH 8) under air.

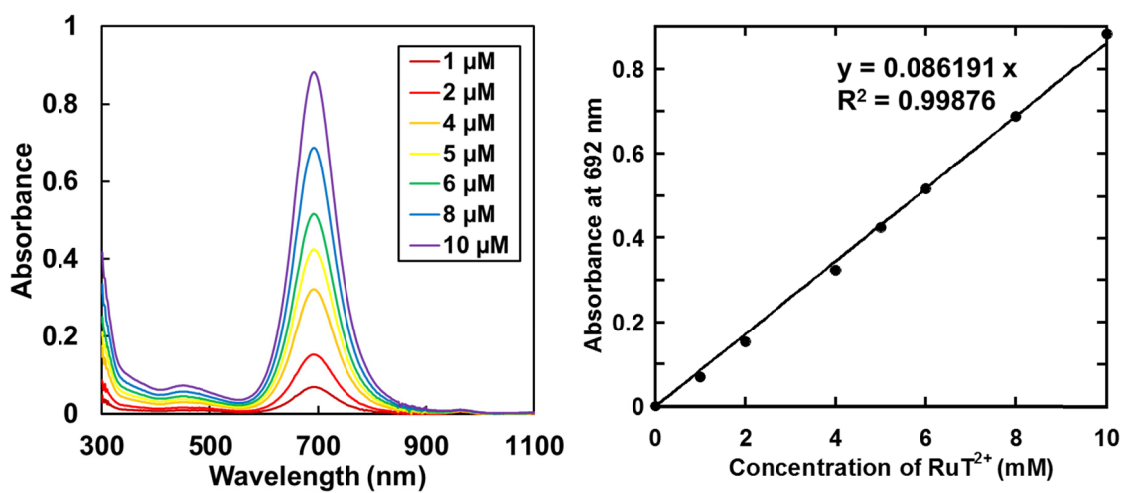


Figure S8. (Left) UV-Vis absorption spectra of $\text{RuT}^{2+}(\text{PF}_6)_2$ in 0.1 M borate buffer (pH 8) at various concentrations in air. (Right) The concentration dependence of absorbance at 692 nm in the concentration range of 0–10 μM , showing that $\text{RuT}^{2+}(\text{PF}_6)_2$ obeys the Beer's law.

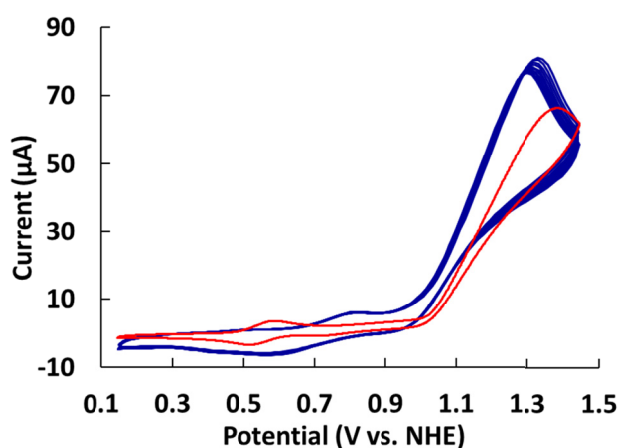


Figure S9. CV of 0.3 mM **RuM** (red) and successive CVs (first 10 cycles) of 0.6 mM **RuT²⁺(PF₆)₂** (blue) in 0.1 M borate buffer (pH 8) with a glassy-carbon working electrode, a Pt wire counter electrode and an Ag/AgCl reference electrode at a scan rate of 0.1 V/s.

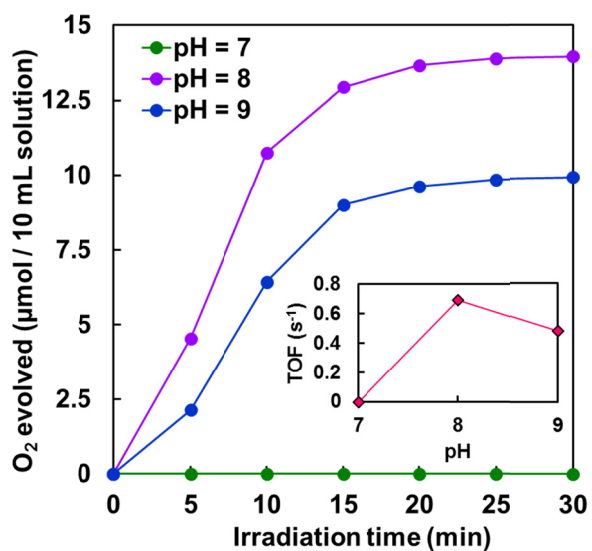


Figure S10. Photochemical oxygen evolution by **RuT²⁺(PF₆)₂** (3 µM) in an aqueous 0.1 M borate buffer containing [Ru(bpy)₃](NO₃)₂ (0.4 mM), and Na₂S₂O₈ (6 mM) under Ar at 20 °C. Inset shows TOF of the photochemical oxygen evolution for 3 µM **RuT²⁺(PF₆)₂** as a function of pH.

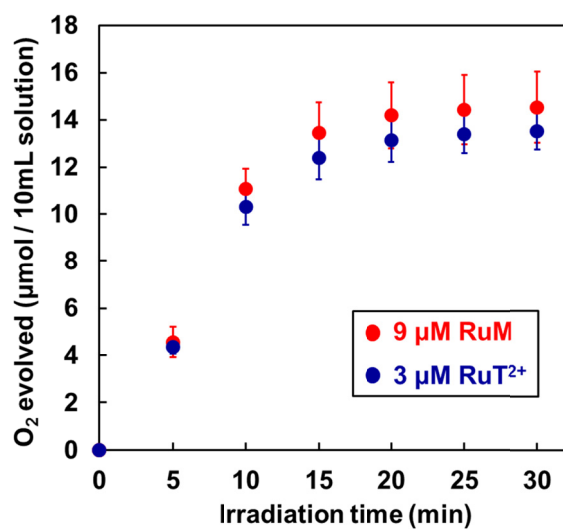


Figure S11. Photochemical oxygen evolution from an aqueous solution containing $[\text{Ru}(\text{bpy})_3](\text{NO}_3)_2$ (0.4 mM), and $\text{Na}_2\text{S}_2\text{O}_8$ (6 mM) in borate buffer (0.1 M, pH 8) under Ar at 20 °C, in the presence of **RuM** (9 μM) and **RuT²⁺**(PF_6)₂ (3 μM). Error bars represent two standard deviations from the mean. The TONs for **RuM** and **RuT²⁺**(PF_6)₂ were determined as 161 ± 17 and 450 ± 26 , respectively.

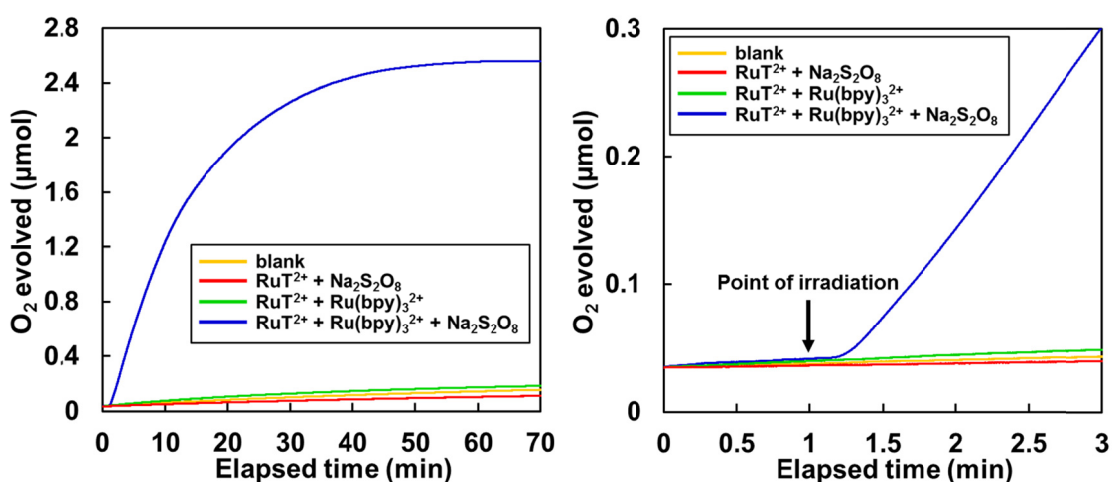


Figure S12. (Left) Photochemical oxygen evolution from 0.1 M pH 8.0 borate buffer solutions of 3 μM $\text{RuT}^{2+}(\text{PF}_6)_2$ + 0.4 mM $[\text{Ru}(\text{bpy})_3](\text{NO}_3)_2$ + 2 mM $\text{Na}_2\text{S}_2\text{O}_8$, blue curve; 3 μM $\text{RuT}^{2+}(\text{PF}_6)_2$ + 0.4 mM $[\text{Ru}(\text{bpy})_3](\text{NO}_3)_2$, green curve; 3 μM $\text{RuT}^{2+}(\text{PF}_6)_2$ + 2 mM $\text{Na}_2\text{S}_2\text{O}_8$, red curve; blank, yellow curve. (Right) A magnified view of left figure over the time range 0-3 min. The black arrow corresponds to the start of light irradiation. The blank slope is due to incidental inclusion of air.

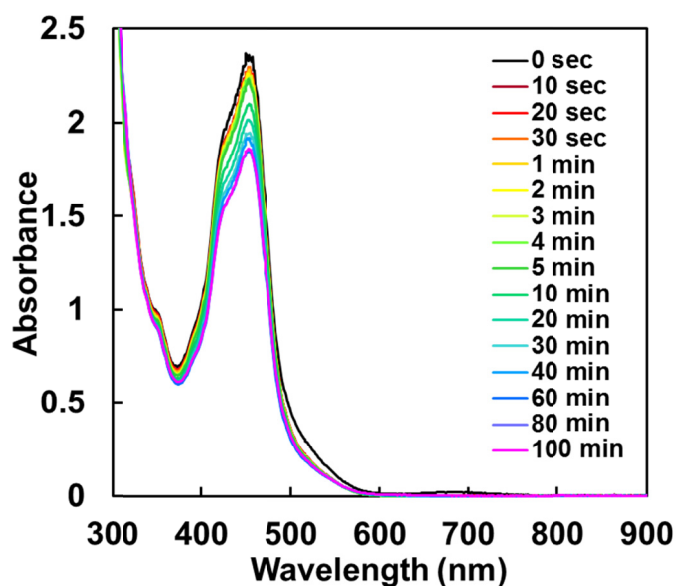


Figure S13. UV-Vis spectral changes during the photolysis of an aqueous borate buffer solution (0.1 M, pH 8) containing $\text{RuT}^{2+}(\text{PF}_6)_2$ (6.7 μM), $[\text{Ru}(\text{bpy})_3](\text{NO}_3)_2$ (0.16 mM) and $\text{Na}_2\text{S}_2\text{O}_8$ (2 mM). Before irradiation, the solution was purged with N_2 for 30 min.

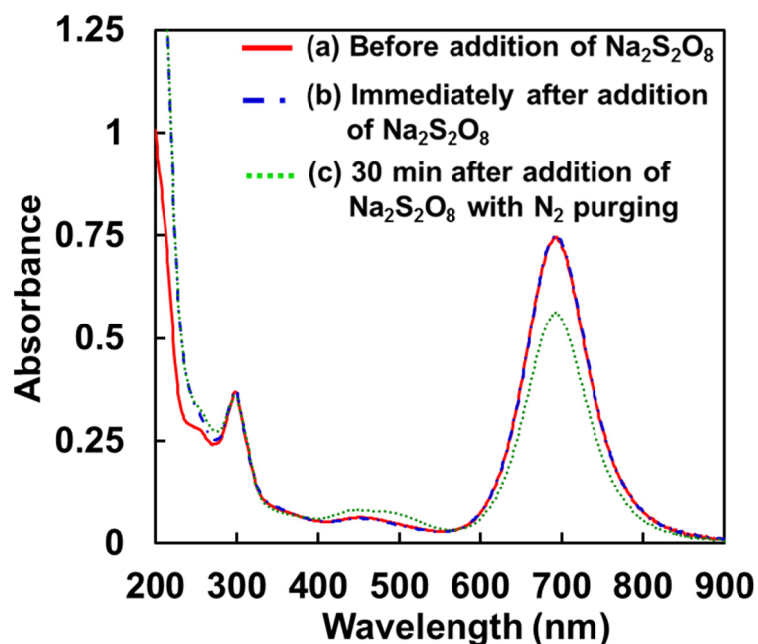


Figure S14. (a) UV-Vis absorption spectrum of $6.7 \mu\text{M RuT}^{2+}(\text{PF}_6)_2$ in borate buffer (0.1 M, pH 8). (b) UV-Vis absorption spectrum of the solution immediately after addition of $\text{Na}_2\text{S}_2\text{O}_8$ (2 mM) to solution (a). (c) UV-Vis absorption spectrum of solution (b) after purging with N_2 for 30 min.

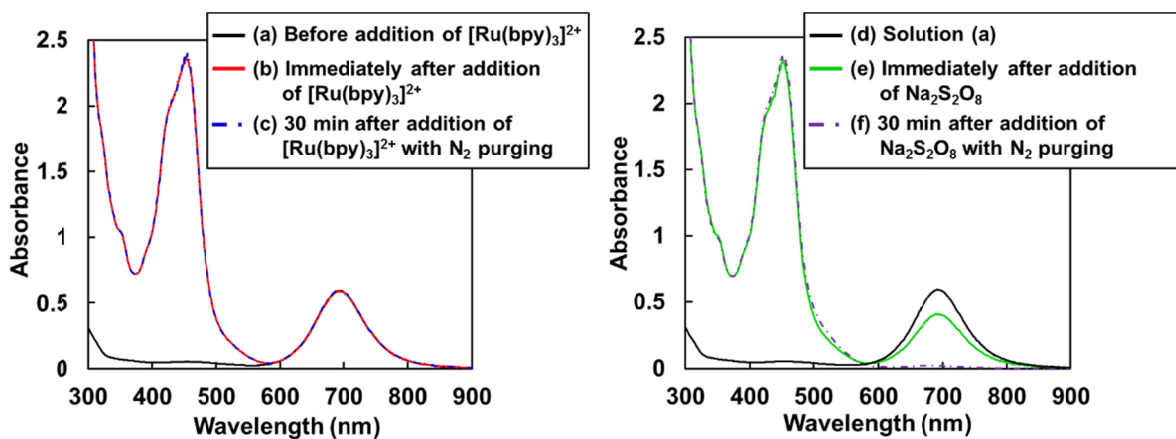


Figure S15. (a and d) UV-Vis absorption spectrum of $6.7 \mu\text{M RuT}^{2+}(\text{PF}_6)_2$ in borate buffer (0.1 M, pH 8). (b) UV-Vis absorption spectrum of the solution immediately after addition of $[\text{Ru}(\text{bpy})_3]^{2+}$ (0.16 mM) to solution (a). (c) UV-Vis absorption spectrum of solution (b) after purging with N_2 for 30 min. (e) UV-Vis absorption spectrum of the solution immediately after addition of $\text{Na}_2\text{S}_2\text{O}_8$ (2 mM) to solution (c). (f) UV-Vis absorption spectrum of solution (e) after purging with N_2 for 30 min.

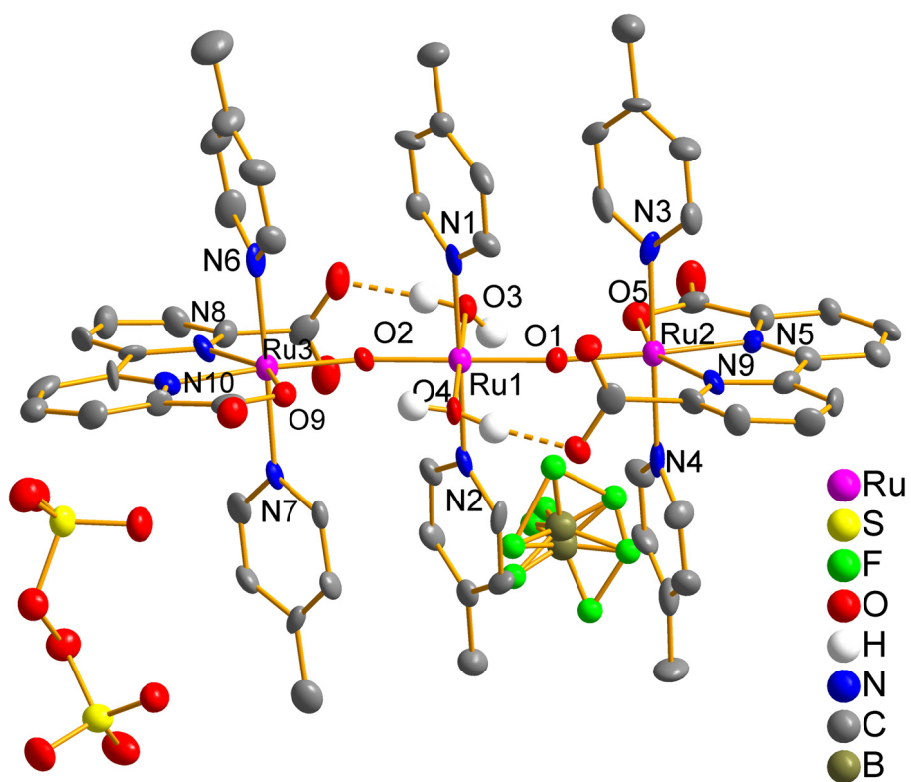


Figure S16. Crystal structure of $[\text{RuT}^{3+}](\text{S}_2\text{O}_8)(\text{BF}_4)\cdot 12\text{H}_2\text{O}$. Hydrogen atoms except for those bonded to oxygen atoms are omitted for clarity. Hydrogen bonds are represented by dotted lines.

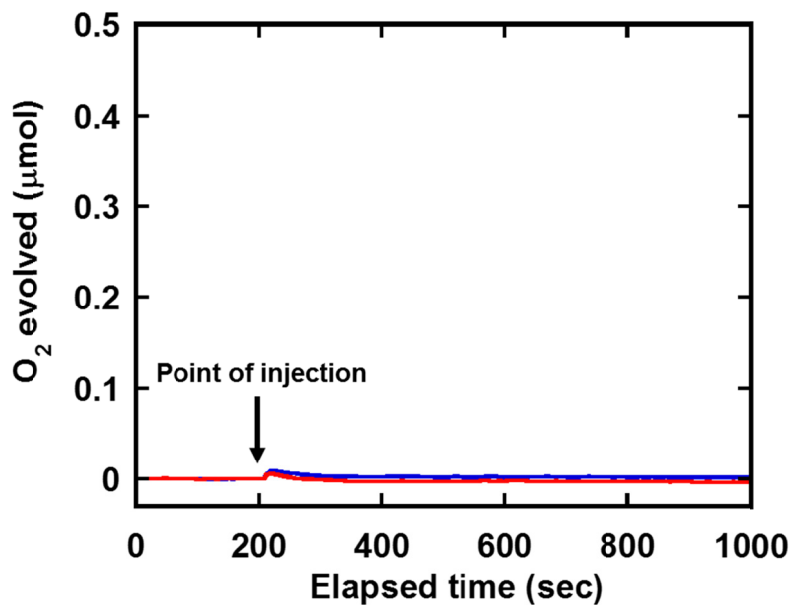


Figure S17. Oxygen evolution from a borate buffer (0.1 M, pH 8) under air at 20 °C with $\text{Na}_2\text{S}_2\text{O}_8$ (1.9 mM) in the presence (red line) or absence (blue line) of $\text{RuT}^{2+}(\text{PF}_6)_2$ (3 μM). The black arrow corresponds to injection of a 250 μL of $\text{RuT}^{2+}(\text{PF}_6)_2$ solution (63 μM).

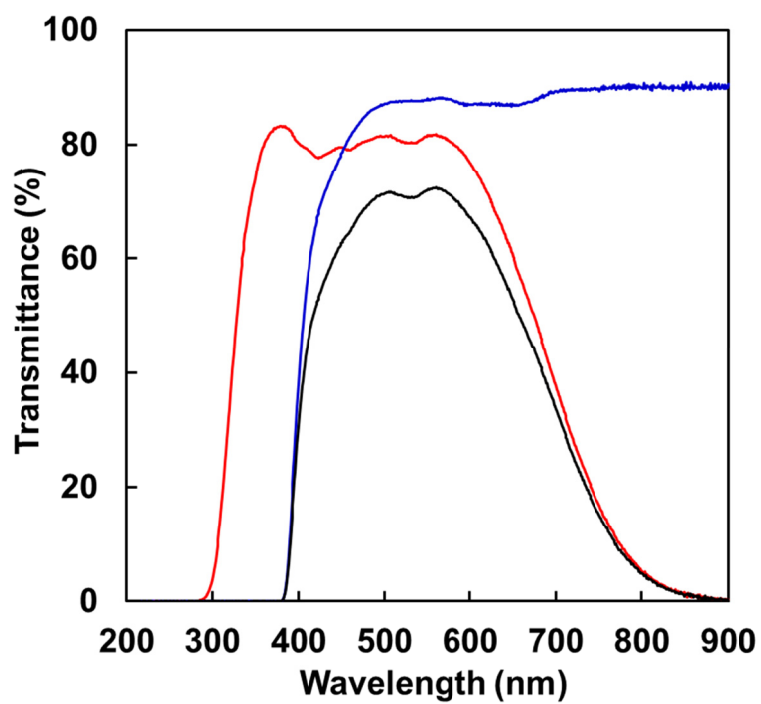


Figure S18. Transmission spectra for a 400 nm long-pass filter (blue), an IR cut filter (red) and a set of both filters (black).

Table S3. Bond distances and the ratios given for the pseudo centrosymmetrically equivalent bonds in the trimeric structure of $[\mathbf{RuT}^{3+}](\text{S}_2\text{O}_8)(\text{BF}_4)\cdot 12\text{H}_2\text{O}$, consistent with a delocalized nature of the mixed-valent $\text{Ru}(3.5+)\text{—O—Ru(IV)—O—Ru}(3.5+)$ triruthenium core.

comparison set number	Left Side		Right Side		centrosymmetry factor
1	Ru1-O2	1.809	Ru1-O1	1.817	0.996
2	Ru1-O3	2.068	Ru1-O4	2.05	1.009
3	Ru1-N2	2.11	Ru1-N1	2.084	1.012
4	Ru3-O2	1.884	Ru2-O1	1.875	1.005
5	Ru3-O9	2.03	Ru2-O5	2.015	1.007
6	Ru3-N8	2.105	Ru2-N9	2.102	1.001
7	Ru3-N7	2.067	Ru2-N3	2.07	0.999
8	Ru3-N6	2.123	Ru2-N4	2.123	1.000
9	Ru3-N10	2.006	Ru2-N5	2.009	0.999

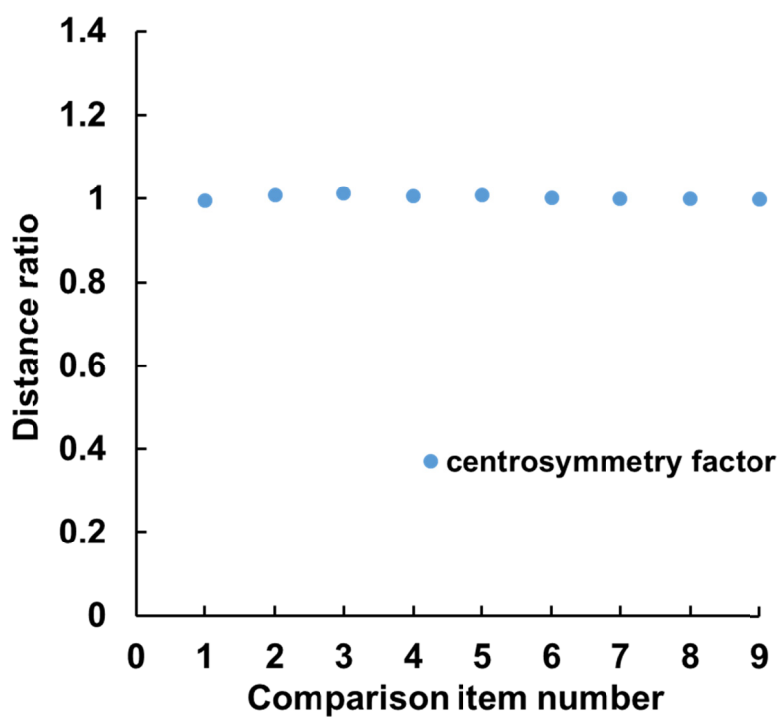


Figure S19. Centrosymmetry factors defined in Table S3 are plotted to show the equivalency of the two terminal Ru(3.5+)-based core.

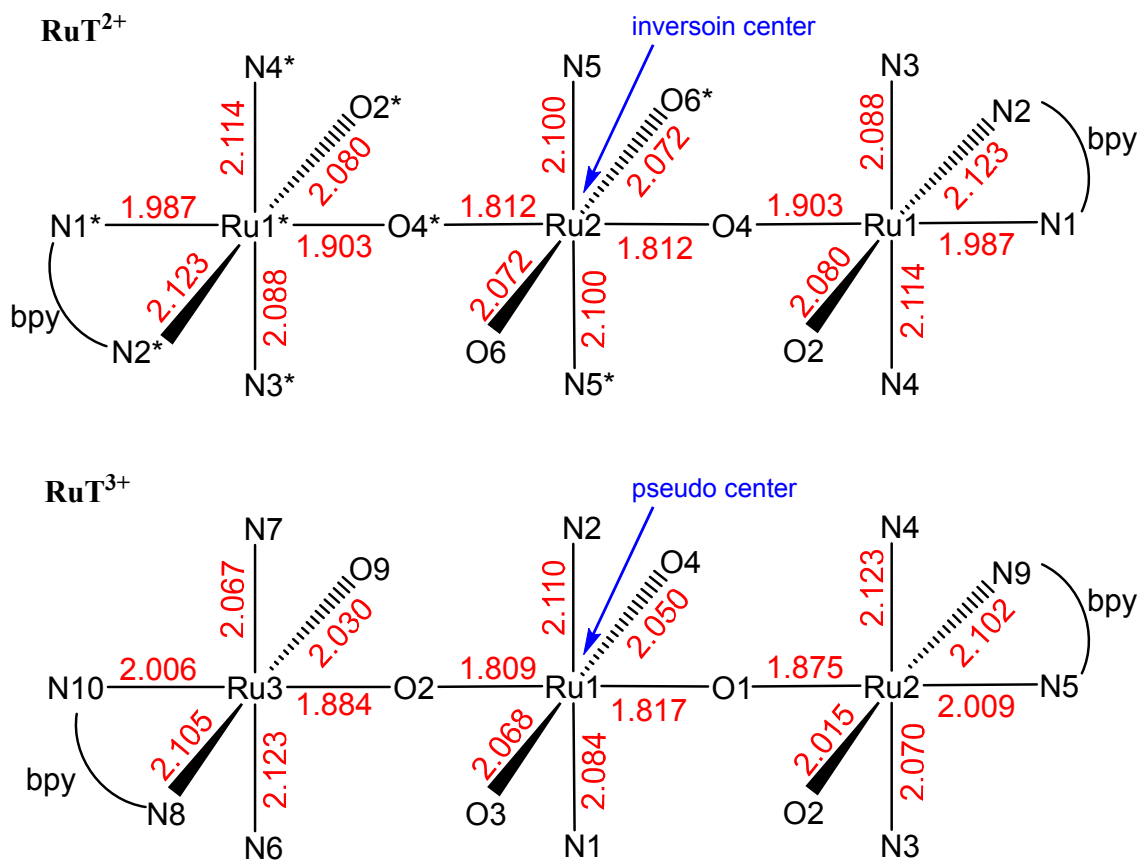


Figure S20. Comparison of the coordinate bond distances between $[\text{RuT}^{2+}](\text{BF}_4)_2 \cdot 8\text{H}_2\text{O}$ and $[\text{RuT}^{3+}](\text{S}_2\text{O}_8)(\text{BF}_4) \cdot 12\text{H}_2\text{O}$ which are in the formal oxidation states of Ru(III)₂Ru(IV) and Ru(III)Ru(IV)₂, respectively, showing a nearly centrosymmetric feature of the latter. This feature is consistent with the delocalized mixed-valence character of the formally Ru(III)Ru(IV)₂ species, providing a description of Ru(3.5⁺)-O-Ru(IV)-O-Ru(3.5⁺) for the latter oxidation state.

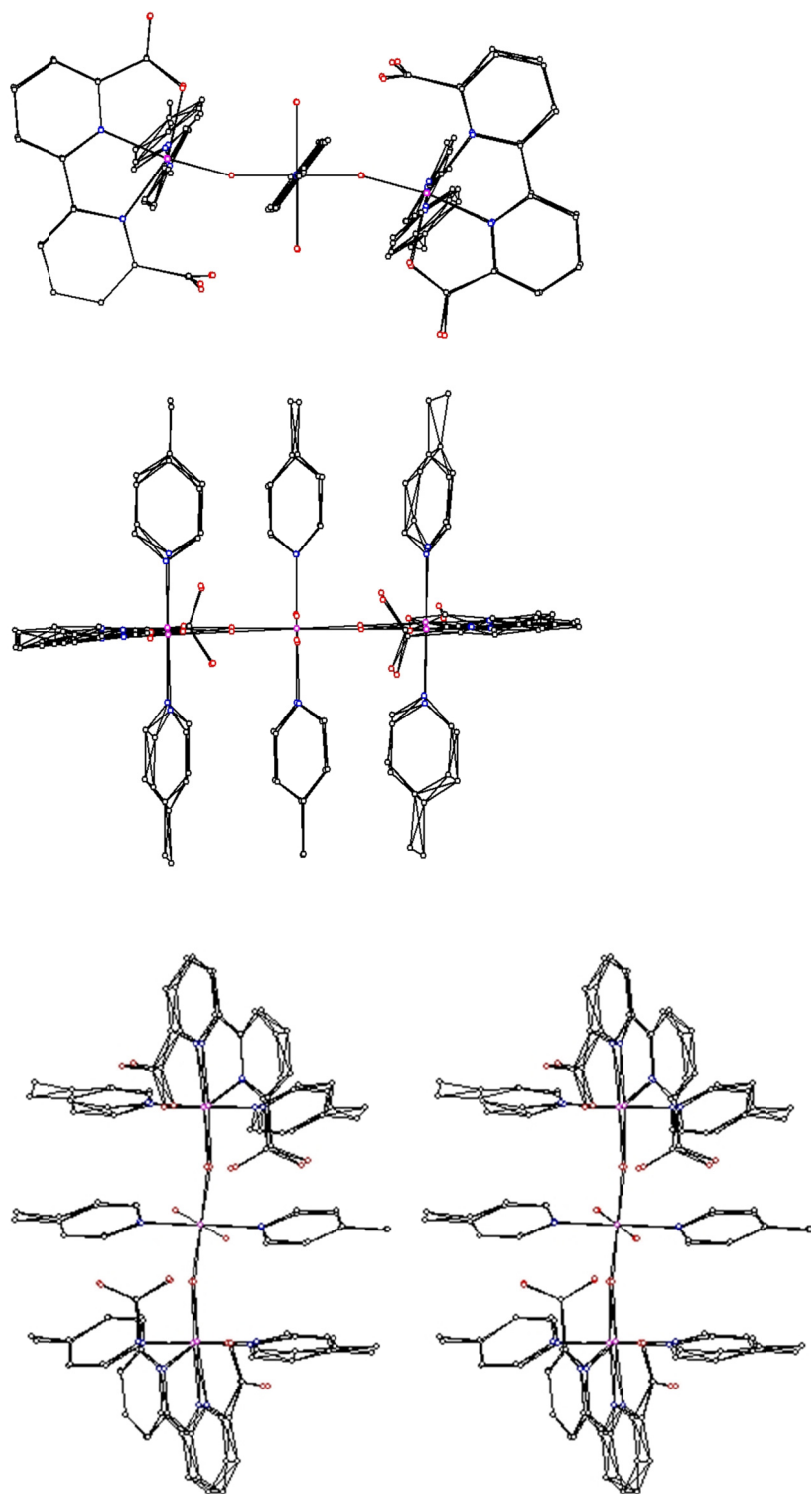


Figure S21. Comparison of trimeric cations of RuT^{2+} and RuT^{3+} by showing the superimposed geometries in three different views, a top view, a side view, and a stereo view (plots generated in KENX).

References

1. L. Duan, A. Fischer, Y. Xu and L. Sun, *J. Am. Chem. Soc.* 2009, **131**, 10397.
2. K. Sakai, Y. Kizaki, T. Tsubomura and K. Matumoto. *J. Mol. Catal.*, 1993, **79**, 141.
3. G. M. Sheldrick, SADABS, Bruker AXS Inc, Madison, WI-53719, USA, 1997.
4. G. M. Sheldrick, SHELXS-97, Program for solution of crystal structures, University of Göttingen, Germany, 1997; G. M. Sheldrick, SHELXL-97, Program for refinement of crystal structures, University of Göttingen, Germany, 1997.
5. K. Sakai, KENX. Graphical User Interface for SHELXL97. Kyushu University, Japan, 2004.
6. CrystalClear and CrystalStructure; Rigaku/MSK: The Woodlands, TX, 2005.
7. G. M. Sheldrick, *Acta Cryst.* 2008, **A64**, 112–122.